Power Electronics and Drives
Volume 8(43), 2023 DOI: 10.2478/pead-2023-0005

Power Electronics and Drives

Mechanical Vibrations Analysis in Direct Drive Using CWT with Complex Morlet Wavelet

Research paper

Dominik Łuczak*

Department of Control and Industrial Electronics, Faculty of Automatic Control, Robotics and Electrical Engineering, Poznan University of Technology, 60-965 Poznań, Poland

Received: 05, November 2022; Accepted: 04, January 2023

Abstract: Modern industrial process and household equipment more often use direct drives. According to European policy, Industry 4.0 and new Industry 5.0 need to undertake the effort required to ensure a sustainable, human-centric, and resilient European industry. One of the main problems of rotating machines is mechanical vibrations that can limit the lifetime of the final product or the machine in which they are applied. Therefore, analysis of vibration in electrical drives is crucial for appropriate maintenance of the machine. The present article undertakes an analysis of vibration measured at the laboratory stand with multiple dominant frequencies in the range 50–500 Hz. The fast Fourier transform (FFT) gives information about the frequency component without its time localisation. While the solution made available by the short-time Fourier transform (STFT) is able to overcome the problem of FFT, it still has limitations, particularly in terms of there being a lacuna in time and frequency localisation; accordingly, the need is felt for other methods that can give a good localisation in time and frequency. In the article, the continuous wavelet transform (CWT) was investigated, which requires selection of the wavelet function (kernel of transformation). The complex Morlet wavelet was selected with description of its central frequency and bandwidth. CWT and STFT time-frequency localisation capabilities were compared to investigate data registered from the direct-drive laboratory stand. CWT gives better frequency localisation than STFT even for the same frequency resolution. Vibration frequencies with near-locations were separated in CWT and STFT joined them into one wide pick. To ensure a good extraction of frequency features in electric drive systems, the author, based on analysing the results of the present study, recommends that CWT with complex Morlet wavelet be used instead of STFT.

Keywords: *CWT • complex Morlet wavelet • STFT • mechanical vibrations • direct drive*

1. Introduction

Modern industrial facilities, households, and electric vehicles are equipped with electrical drives (Nowopolski et al., 2017; Szabat et al., 2020; Urbanski and Janiszewski, 2021) and mechanical working parts. Those mechatronics parts have a limited life time that decreases if not maintained correctly. Therefore, appropriate monitoring of electromechanical behaviour is crucial for extension of their lifetime. In addition, European policy has highlighted multiple aspects concerning this direction. The European industry 4.0 'describes the organisation of production processes based on technology and devices autonomously communicating with each other along the value chain' (Smit et al., 2016; Teixeira and Tavares-Lehmann, 2022). The next step in European policy is Industry 5.0 (Directorate-General for Research and Innovation [European Commission] et al., 2021), where key aspects, pertaining to the sustainability, human-centricity, and resilience of the European industry, are discussed. Two main aspects can be delivered: first, long usage of the mechatronic system with appropriate maintenance, and second, autonomous communication in the monitoring and maintenance process.

A popular method of investigation is based on frequency analysis of rotating machines (Brock et al., 2016; Han et al., 2022; Łuczak, 2021; Miletic et al., 2022; Peeters et al., 2018; Pindoriya et al., 2018; Ramteke et al., 2022;

* Email: dominik.luczak@put.poznan.pl

Strakosch et al., 2021; Wszołek et al., 2020). The option that is mostly used is the fast Fourier transform (FFT) based on the radix-2 (Cooley and Tukey, 1965) or radix-4 algorithm (Corinthios et al., 1975); however, very often, there is no information available concerning the question which FFT algorithm has been employed (Duda et al., 2021; Gong and Deng, 2022). The limitation of FFT analysis is the length of time window. Good frequency resolution requires a large number of samples and is related by $f_{res} = f_s/N$, where *N* indicates the signal length of the samples and f_s the sampling frequency. Another limitation is the lack of information concerning frequency change over time. This problem can be overcome by short-time Fourier transform (STFT), which performs FFT on overlapping time windows. However, this does not solve the frequency resolution problem because a long time window will lead to poor localisation of frequencies in time. Instead of time-frequency analysis, time-scale analysis can be applied to get good localisation both in time and scale (frequency). Continuous wavelet transform (CWT) allows for time-scale analysis and will be presented in the forthcoming section.

The frequency components of the analysed signal, as ascertained based on the application of FFT, can be seen in Figure 3 (right). However, this analysis does not provide an answer to the question of whether this is a single occurrence within the signal or if this component appears, as is possible, several times within the time domain. The prospect of discovering an answer to the above question brings out the need for a time-frequency analysis. However, when STFT was used, some frequencies that were seen in FFT were blurred in STFT (Figure 5). The author searches for other tools that can be used for this purpose to have good time and frequency localisation with less blurred frequency data. The CWT with an appropriate selected mother wavelet and appropriate selected parameters of the wavelet gives satisfactory results. The use of CWT with complex Morlet wavelet gives better results (Figure 7) than STFT.

2. Short-Time Fourier Transform

The STFT is a method that allows transforming a one-dimensional function of time into a two-dimensional function of frequency and time. The method uses a fixed-length time window, which is shifted through the analysed signal. For each time interval, an FFT is calculated. The process is repeated in the next collection of samples. The shift of time window in samples is a parameter that can be chosen. The time shift can also be considered as an overlap of a subsequent time window with the previous one. In the present study, the calculation of FFT was done after each new sample, which means K–1 overlap of the signal, where K is the time window length in samples. It means that the step size is equal to one sample. By default, the shape of the time window is a rectangle; however, other known shapes of window are recommended to be used to reduce spectrum leak-out. In the present study, the Keiser shape of the window was used. The STFT is calculated as follows:

$$F(\tau, f) = \int_{-\infty}^{+\infty} f(t) \cdot w(t-\tau) e^{-j2\pi f \cdot t} dt \tag{1}$$

where τ indicates time shift parameter, f frequency parameter, *w(t)* fixed-length time window, *f(t)* the function that is analysed, and *F* the result coefficients.

The resolution in time depends on the step size, which, in the present study, was selected as a single sample. However, the resolution in frequency is calculated in the same way as for FFT. Therefore, the length of the fixed-time window will decide the frequency resolution as follows: $f_{res} = f_s/K$, where *K* indicates time window length in samples and f_s the sampling frequency. Selection of a long time window is appropriate for good frequency localisation, but the time localisation will be poor. In contrast, selection of a short time window will give poor frequency localisation, although time localisation will increase. Therefore, the selection of *w(t)* length is a compromise between good localisation in time or frequency. Additionally, application of technique of frequency resolution increment is made possible by extending the time window length by the lengths of samples whose value is zero. In the paper, *K* was equal to 1,024 samples (0.1024 s) and an additional 1,024 zero samples were added. This gives an appropriate time localisation and frequency resolution given by $f_{res} = \frac{10{,}000\,Hz}{1024+1024} = 4.8828\,Hz$.

3. Continuous Wavelet Transform

The CWT is a method that allows transforming a one-dimensional function of time into a two-dimensional function of scale and time. The main advantage of this approach is the scaling of the time window. This allows the precise selection of frequencies of the signal based on the scale of the window, which can be fitted to a period of the main signal component. The single period of the low-frequency and high-frequency components requires application of different time window sizes to capture it for all periods. CWT is an integral transform with a selectable kernel function Ψ. CWT is calculated as follows:

$$W(a,b) = \frac{1}{\sqrt{a}} \int_{-\infty}^{+\infty} f(t) \cdot \overline{\Psi}\left(\frac{t-b}{a}\right) dt \tag{2}$$

where *a* indicates scale parameter, *b* shift parameter, $\overline{\Psi}$ complex-conjugate of the mother wavelet function, and *f(t)* the function that is analysed, namely W result coefficients. A detailed explanation of scale and shift influence can be found in Gao and Yan (2011). A mother wavelet function can be any function that satisfies kernel conditions, and therefore, answering to this description, Daubechies wavelets can be found in the literature (Daubechies, 1988), as also Gaussian wavelets, Shannon wavelets, Morlet wavelets, or complex Morlet wavelets (Teolis, 1998). The complex wavelet function Ψ_M is defined by:

$$\Psi_M(t) = \frac{1}{\sqrt{\pi f_b}} e^{j2\pi f_c t} e^{\frac{-t^2}{f_b}} \tag{3}$$

where f_c denotes the centre frequency, and f_b the variance (bandwidth). The kernel of Ψ_M has two main parts, where the first is $e^{j2\pi f_c t}$ that by Euler's formula gives $\cos(2\pi f_c t) + j\sin(2\pi f_c t)$ and is equivalent to the Fourier transform kernel. The second part is e^{-t^2/f_b}, which can be treated as a time window shape equivalent to an envelope. As an example, a complex Morlet wavelet in the time and frequency domain is shown in Figure 1. The parameter f_c is exactly the maximum frequency and f_b is the inverse of the spectral width (the inverse of the variance in the frequency domain). The magnitude spectrum calculated of the real and imaginary parts are identical for the complex Morlet wavelet.

The CWT result is a function of *a*, scale, and *b*, shift parameter, and therefore, it can be called a time-scale analysis. However, it is more useful to transform it from a time scale to a time frequency (time-pseudo frequency). The transformation from scale to pseudo-frequency is done by:

$$f_{\text{pseudo}} = \frac{f_{\text{middle wavelet}}}{a \cdot dt} \tag{4}$$

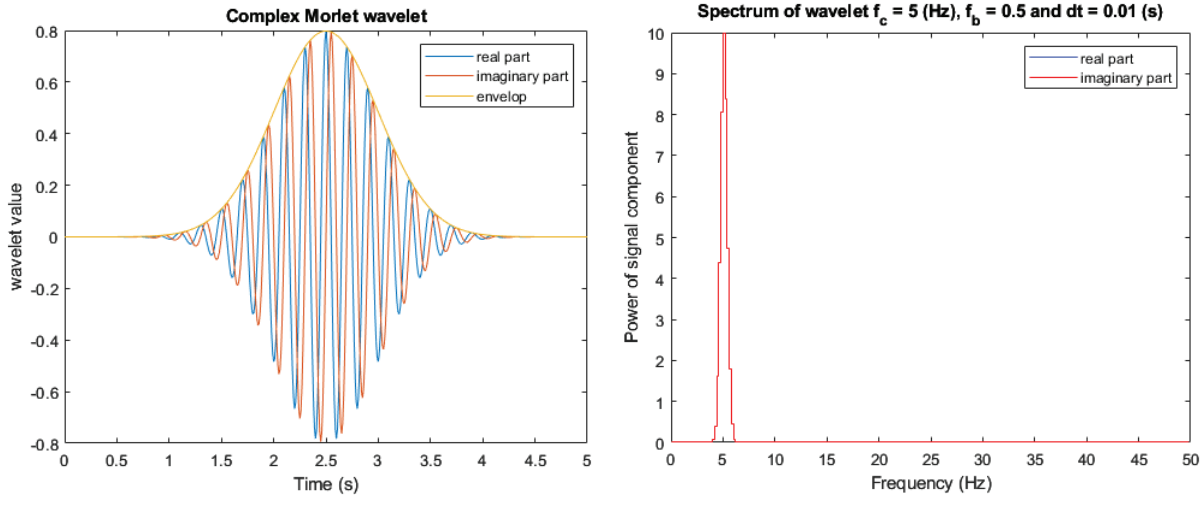

Fig. 1. Complex Morlet wavelet. Time domain with a shift of 2.5 s (left) and a magnitude spectrum of the real and imaginary parts of the wavelet (right).

where $f_{\text{middle wavelet}}$ is the dominant frequency of the wavelet function and *dt* is the sampling time. The spectrum of wavelet function can contain more than one frequency component and only one dominant frequency is selected, and the remaining components are omitted; therefore, it is called pseudo-frequency. The dominant middle frequency of the complex Morlet wavelet is equal to f_c. The resolution of pseudo-frequency depends directly on the selected scale *a* by application to Eq. (4). To compare STFT and CWT with the Morlet wavelet, the scale *a* was calculated after transformation of Eq. (4) into Eq. (5). The values of f_{pseudo} were chosen as the same frequencies as in STFT.

$$a = \frac{f_{\text{middle wavelet}}}{f_{\text{pseudo}} \cdot dt} \tag{5}$$

4. Direct Drive Laboratory Stand and Data Analysis

The direct drive laboratory stand is equipped with a Permanent Magnet Synchronous Motor (PMSM) electric motor, a control board with a Analog Devices Inc. SHARC® signal microprocessor, a Pulse-Width Modulation (PWM) transistor inverter, and oscilloscopes. Raw measurement data can be collected in the microprocessor internal memory or through analogue outputs registered by the oscilloscope. In the present study, the registration in the internal memory of the microprocessor was used. The laboratory stand is presented in Figure 2. Analysis was done based on mechanical position θ_M measurements with excitation of i_q^{ref} current. The shape of the excitation signal was linear chirp (Luczak and Zawirski, 2015) in range of 50–500 Hz. Current i_q^{ref} forced the direct drive to vibrate in the given frequency range. Data were collected with a sampling frequency f_s = 10,000 Hz. The measured velocity and its spectrum calculated by FFT are presented in Figure 3. The main frequencies of the vibrations are as follows: 80 Hz, 140 Hz, 156 Hz, 180 Hz, 277 Hz, and 400 Hz. Frequency analysis is a powerful tool; however, it does not give information on the time localisation of each frequency.

The data collected and presented in Figure 3 were transformed into time-frequency domain using the STFT method (Figure 4 [left] and Figure 5). The time window overlaps with the previous time window by window length (1,024 samples) minus 1. The frequency resolution of STFT is 4.88 Hz by the zero padding method. The result of STFT is the complex number coefficients of time and frequency. The modulus of complex numbers obtained resultant to the STFT is presented in Figures 4 (left) and 5. As a result of the STFT, a 3D chart is obtained (Figure 4 [left]), where the X-axis is time, the Y-axis is the frequency, and the Z-axis is modulus. View in the X–Y (time-frequency) axis allows analysing change of signal frequency components with respect to time and view in the Y–Z (frequency-module) axis allows investigating the frequency components. Time and frequency localisation is fair; however, in the Y–Z (frequency-module) axis, only frequencies with a wider frequency gap can be found for viewing. The main frequencies are as follows: 80 Hz, 180 Hz, 277 Hz, and 400 Hz.

The CWT result is similar to that obtained with STFT and is represented as a 3D graph in Figure 4 (right), where the X-axis is time, the Y-axis is the pseudo-frequency, and the Z-axis is modulus. The same raw data were transformed to time-scale domain by CWT with complex Morlet wavelet with f_b = 4 and f_c = 5, and scale was calculated by Eq. (4) from the given frequencies having the range 0.1–500.0 Hz with a 2 Hz step. The CWT are complex number coefficients of time and scale. However, scale can be transformed to f_{pseudo} by Eq. (4), which gives a time-frequency chart. The modulus of the complex numbers of CWT result is presented in Figure 6. Time localisation obtained by CWT is similar to that by STFT. On the other hand, the frequency localisation obtained by CWT is better than STFT, as shown in Figure 6. The Y–Z axis view allows reading all main frequencies, which are as follows: 80 Hz, 140 Hz, 156 Hz, 180 Hz, 277 Hz, and 400 Hz. The frequency localisation of CWT is as good as that of FFT.

A better frequency localisation of the CWT can be achieved even if the frequency resolution of both methods is the same. Figures 4 and 7 (right) present the results of CWT analysis conducted with frequencies in the range 0.1–500.0 Hz with a 4.88 Hz step. Due to the worse frequency resolution, the frequency of 156 Hz is not visible and is part of a wide 180 Hz peak; however, 140 Hz is still visible.

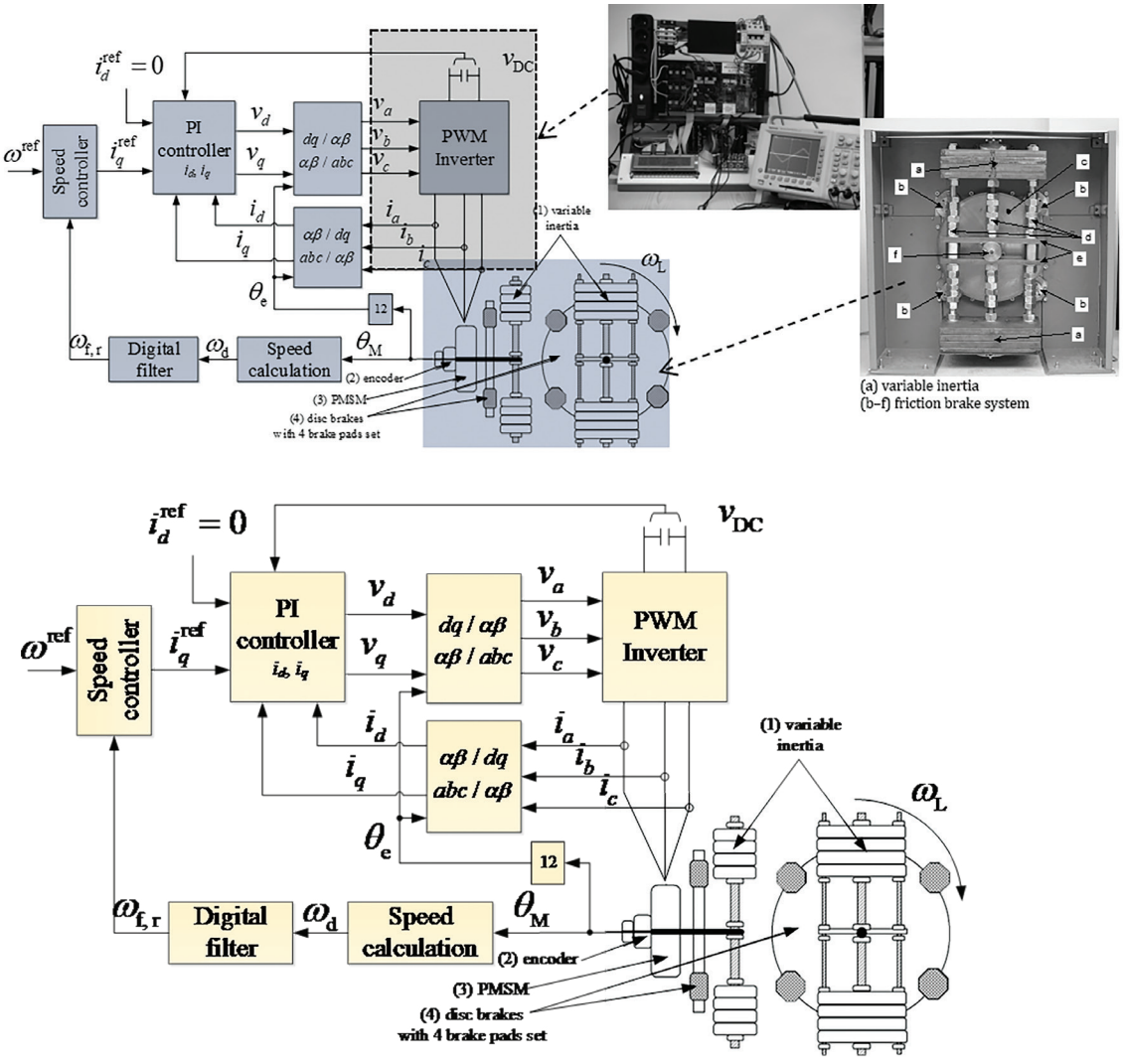

Fig. 2. Direct drive laboratory stand and control schematic.

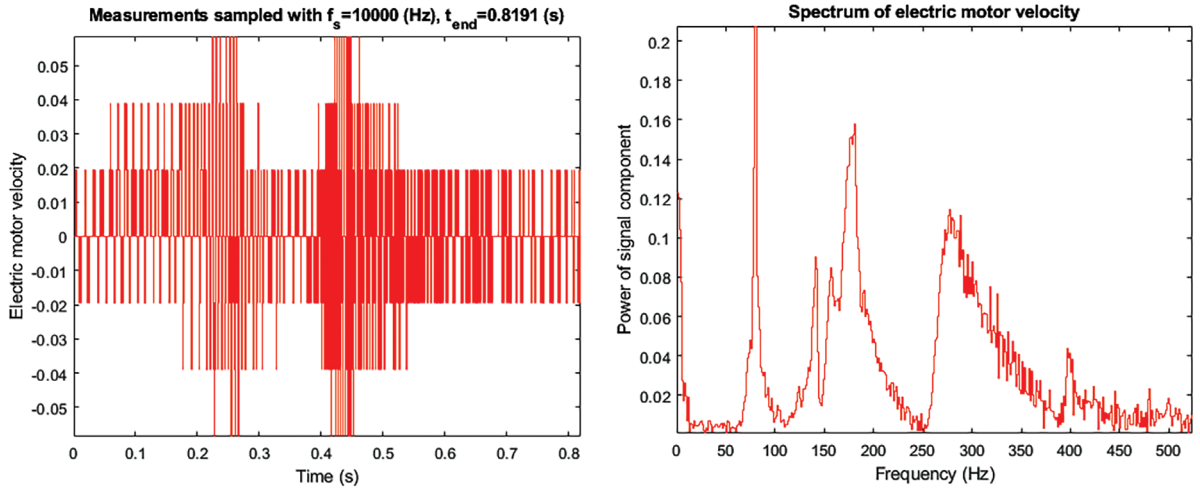

Fig. 3. Measured motor velocity (left) and its spectrum calculated by FFT (right). FFT, fast Fourier transform.

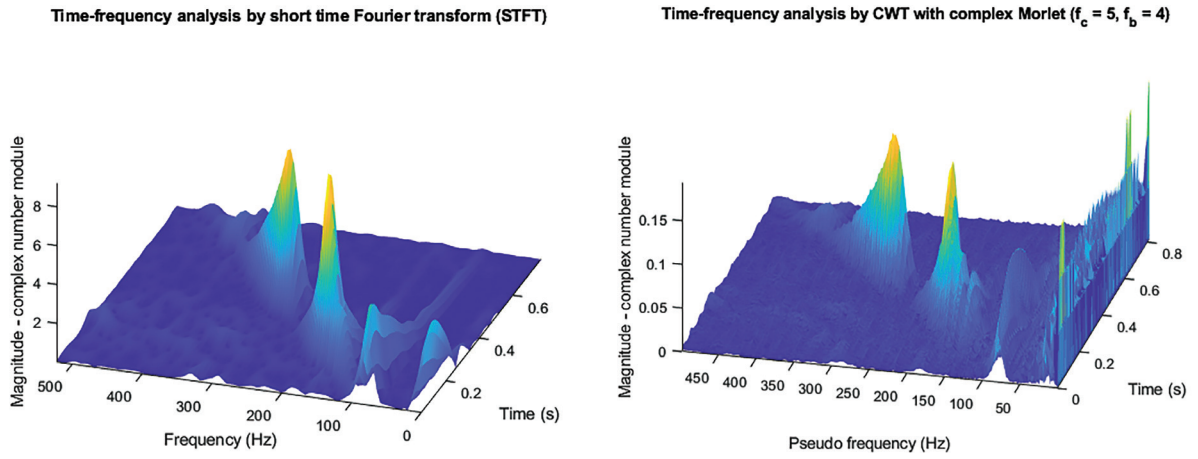

Fig. 4. STFT analysis (4.88 Hz resolution) of the measured motor velocity (left) and CWT analysis (4.88 Hz resolution) of the measured motor velocity (right). CWT, continuous wavelet transform; STFT, short-time Fourier transform.

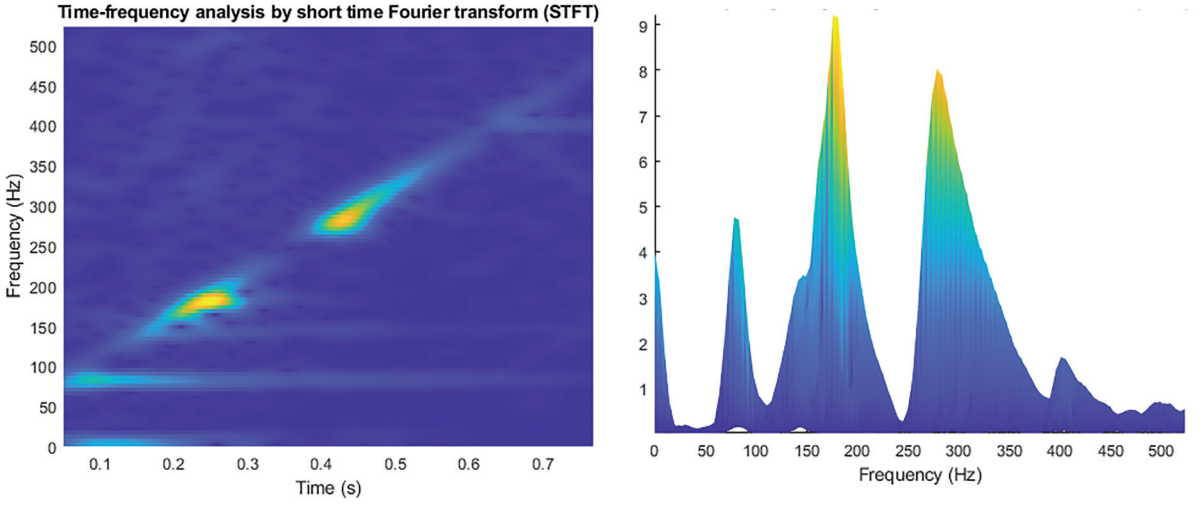

Fig. 5. STFT analysis (4.88 Hz resolution) of the measured motor velocity (left) and its Y–Z axis view (right). STFT, short-time Fourier transform.

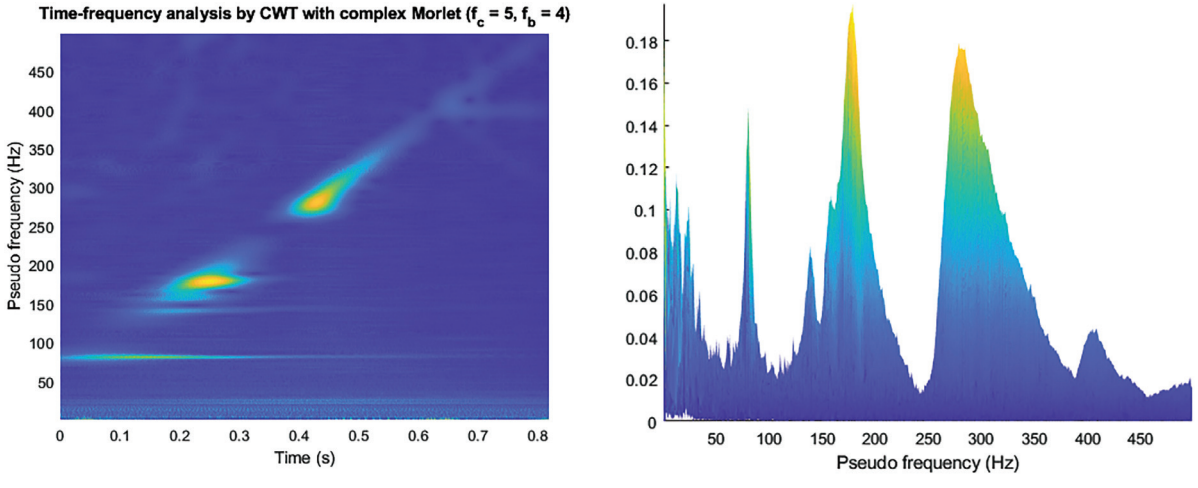

Fig. 6. CWT analysis (2 Hz resolution) of measured motor velocity (left) and its view of the Y–Z axis (right). CWT, continuous wavelet transform.

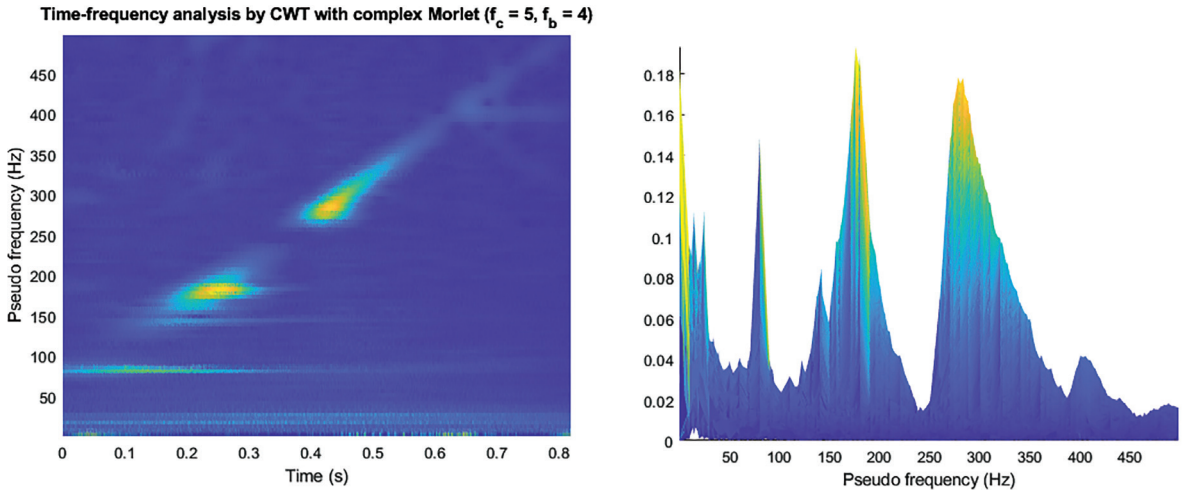

Fig. 7. CWT analysis (4.88 Hz resolution) of the measured motor velocity (left) and its view of the Y–Z axis (right). CWT, continuous wavelet transform.

5. Discussion

Measurement data collected on a direct-drive laboratory stand were investigated by FFT, STFT, and CWT. FFT gives a good frequency localisation, although it does not facilitate ascertainment of the occurrence times. The FFT is appropriate if only information about frequency components is requested. However, information about time localisation is not present. This problem is solved by the time-frequency analysis. Easy-to-apply STFT with maximum time window overlap can give good time localisation; however, it has the disadvantage of frequency localisation. The STFT uses FFT on smaller fixed-length time windows, which leads to blurred frequency data. Therefore, a long fixed-length time window in STFT will give less blurred magnitude than a shorter fixed-length time window in STFT. Selection of time window length constitutes a trade-off between good localisation in time or frequency. If time window will be the same length as in FFT, it will give the same frequency data; however, there will be no time localisation. The key issue of STFT is fixed-length time window to calculate $F(\tau, f)$. Another aspect is that *F* is calculated from a given time window for all *f,* which leads to new data on the Y–Z axis at the X-axis equal to τ. The author searches for other tools that can be used for this purpose to have good time and frequency localisation with less blurred frequency data. Accordingly, the author proposes usage of CWT with complex Morlet wavelet, which gives good localisation in time and frequency. The CWT uses a varied-length time window (scaling of wavelet), which leads to less blurred frequency data. For each pseudo-frequency (scale *a*), a different wavelet length is used. If the scale *a* factor is large, the time window (wavelet) is long, which is appropriate for low-frequency components; on the other hand, if the scale *a* factor is small, the time window (wavelet) is short, which is appropriate for high-frequency components. The result of CWT is $W(a,b)$. The convolution operation in time is used with a scaled wavelet corresponding to each scale a (pseudo-frequency), which leads to new data on the X–Z axis at Y-axis equal to scale a; accordingly, the frequency resolution can be selected based on scale a.

Other aspects of STFT and CWT include computational complexity, which depends on selected parameters and algorithms used for FFT. Computational complexity of STFT depends on: (1) selection of FFT algorithm e.g. radix-2 or radix-4, (2) length of fixed-time window, and (3) overlap of next time window with the previous one. The overlap of the long time window with K-1 samples will impose greater requirements on hardware in comparison with a similar phenomenon observed in the case of the shorter time window, which is characterised by fewer overlapped samples. The computational complexity of CWT depends on: (1) selection of convolution algorithm in time $f(t) * \overline{\Psi}(t/a)$ or frequency equivalent $IFFT\{FFT\{f(t)\} \cdot FFT\{\overline{\Psi}(t/a)\}\}$ with fast inverse Fourier transform (IFFT), (2) shape and length of the mother wavelet, and (3) number of selected scales for which CWT will be calculated. The computational complexity test was performed in the MathWorks Matlab R2022b installed on a laptop (i7-4720HQ CPU up to 3.60 GHz, total cores: 4, total threads: 8; 16 GB RAM; Samsung SSD 850 PRO 256 GB). The time of STFT and CWT calculation was measured for a resolution of 4.88 Hz. CWT was calculated using the *cwt()* function defined in the MathWorks Wavelet Toolbox ver. 6.2, and STFT was calculated using the *stft()* function defined in the

MathWorks Signal Processing Toolbox ver. 9.1. STFT was calculated in a time of about 0.2 s and CWT in a time of approximately 4.9 s. STFT was calculated about 25 times faster than CWT. The second test was performed for Python version 3.8.2 with SciPy and PyWavelets (Lee et al., 2019) software module. CWT was calculated using the *pywt.cwt()* function defined in PyWavelets ver. 1.1.1, and STFT was calculated using the *scipy.signal.stft()* function defined in SciPy ver. 1.7.1. STFT was calculated in a time of about 0.45 s and CWT in a time of approximately 5.6 s using time convolution and 0.8 s using frequency domain convolution. CWT implementation in PyWavelets using frequency domain convolution is about seven times faster than that using time convolution.

STFT and CWT methods were examined on real measurements' data. The methods were compared in the region of interest from 50 Hz to 500 Hz. The selection of $f_b = 4$ and $f_c = 5$ has a crucial impact on the time-frequency localisation of the analysed signal. The author has selected both parameters of complex Morlet wavelet to achieve good localisation in time and pseudo-frequency.

Acknowledgements

This work has been funded by the Poznan University of Technology under the project 0214/SBAD/0236.

References

Brock, S., Łuczak, D., Nowopolski, K., Pajchrowski, T. and Zawirski, K. (2016). Two Approaches to Speed Control for Multi-Mass System with Variable Mechanical Parameters. *IEEE Transactions on Industrial Electronics*, 99, pp. 1–1. doi: 10.1109/TIE.2016.2598299.

Cooley, J. W. and Tukey, J. W. (1965). An Algorithm for the Machine Calculation of Complex Fourier Series. *Mathematics of Computation*, 19(90), pp. 297–301. doi: 10.2307/2003354.

Corinthios, M. J., Smith, K. C. and Yen, J. L. (1975). A Parallel Radix-4 Fast Fourier Transform Computer. *IEEE Transactions on Computers*, C-24(1), pp. 80–92. doi: 10.1109/T-C.1975.224085.

Daubechies, I. (1988). Orthonormal Bases of Compactly Supported Wavelets. *Communications on Pure and Applied Mathematics*, 41(7), pp. 909–996. doi: 10.1002/cpa.3160410705.

European Commission and Directorate-General for Research and Innovation and Breque, M and De Nul, L and Petridis, A (2021). *Industry 5.0: Towards A Sustainable, Human Centric and Resilient European Industry*. LU: Publications Office of the European Union. Available at: https://data.europa.eu/doi/10.2777/308407 [Accessed: 27 Oct. 2022].

European Parliament and Directorate-General for Internal Policies of the Union and Carlberg, M and Kreutzer, S and Smit, J and Moeller, C (2016). *Industry 4.0, European Parliament, Policy Department A: Economic and Scientific Policy*. Available at: https://www.europarl.europa.eu/RegData/etudes/STUD/2016/570007/IPOL_STU(2016)570007_EN.pdf.

Duda, T. Mülder, C., Jacobs, G., Hameyer, K., Bosse, D. and Cardaun, M. (2021). Integration of Electromagnetic Finite Element Models in a Multibody Simulation to Evaluate Vibrations in Direct-Drive Generators. *Forschung im Ingenieurwesen*, 85(2), pp. 257–264. doi: 10.1007/s10010-021-00472-z.

Gao, R. X. and Yan, R. (2011). Continuous Wavelet Transform. In: R. X. Gao and R. Yan, eds., *Wavelets: Theory and Applications for Manufacturing*. Boston, MA: Springer US, pp. 33–48. doi: 10.1007/978-1-4419-1545-0_3.

Gong, C. and Deng, F. (2022). Design and Optimization of a High-Torque-Density Low-Torque-Ripple Vernier Machine Using Ferrite Magnets for Direct-Drive Applications. *IEEE Transactions on Industrial Electronics*, 69(6), pp. 5421–5431. doi: 10.1109/TIE.2021.3090714.

Han, T., Ding, L., Qi, D., Li, C., Fu, Z. and Chen, W. (2022). Compound faults diagnosis method for wind turbine mainshaft bearing with Teager and second-order stochastic resonance. *Measurement*, 202, p. 111931. doi: 10.1016/j.measurement.2022.111931.

Lee, G. R., Gommers, R., Waselewski, F., Wohlfahrt, K. and O'Leary, A. (2019). PyWavelets: A Python

Package for Wavelet Analysis. *Journal of Open Source Software*, 4(36), p. 1237. doi: 10.21105/joss.01237.

Łuczak, D. (2021). Nonlinear Identification with Constraints in Frequency Domain of Electric Direct Drive with Multi-Resonant Mechanical Part. *Energies*, 14(21), p. 7190. doi: 10.3390/en14217190.

Luczak, D. and Zawirski, K. (2015). Parametric identification of multi-mass mechanical systems in electrical drives using nonlinear least squares method. In: *IECON 2015 – 41st Annual Conference of the IEEE Industrial Electronics Society*, Yokohama, Japan, 9–12 November 2015, pp. 004046–004051. doi: 10.1109/IECON.2015.7392730.

Miletic, F. M., Jovancic, P. D., Milovancevic, M. D., Tanasijevic, M. L. and Djenadic, S. P. (2022). Determining the Impact of Cutting Elements State on the Bucket–Wheel Excavator Vibration and Energy Consumption. *Journal of Vibration Engineering and Technologies*, 10(5), pp. 1765–1777. doi: 10.1007/s42417-022-00482-3.

Nowopolski, K., Wicher, B., Łuczak, D. and Siwek, P. (2017). Recursive neural network as speed controller for two-sided electrical drive with complex mechanical structure. In: *2017 22nd International Conference on Methods and Models in Automation and Robotics (MMAR)*, Miedzyzdroje, Poland, 28–31 August 2017, pp. 576–581. doi: 10.1109/MMAR.2017.8046892.

Peeters, C., Guillaume, P. and Helsen, J. (2018). Vibration-Based Bearing Fault Detection for Operations and Maintenance Cost Reduction in Wind Energy. *Renewable Energy*, 116, pp. 74–87. doi: 10.1016/j.renene.2017.01.056.

Pindoriya, R. M., Mishra, A. K., Rajpurohit, B. S. and Kumar, R. (2018). An analysis of vibration and acoustic noise of BLDC motor drive. In: *2018 IEEE Power and Energy Society General Meeting (PESGM)*. *2018 IEEE Power and Energy Society General Meeting (PESGM)*, Portland, OR, USA, 5–10 August 2018, pp. 1–5. doi: 10.1109/PESGM.2018.8585750.

Ramteke, S. M., Chelladurai, H. and Amarnath, M. (2022). Diagnosis and Classification of Diesel Engine Components Faults Using Time–Frequency and Machine Learning Approach. *Journal of Vibration Engineering and Technologies*, 10(1), pp. 175–192. doi: 10.1007/s42417-021-00370-2.

Strakosch, F., Nikoleizig, H. and Derbel, F. (2021). Analysis and evaluation of vibration sensors for predictive maintenance of large gears with an appropriate test bench. In: *2021 IEEE International Instrumentation and Measurement Technology Conference (I2MTC)*, Glasgow, UK, 17–20 May 2021, pp. 1–6. doi: 10.1109/I2MTC50364.2021.9460047.

Szabat, K., Wróbel, K., Dróżdż, K., Janiszewski, D., Pajchrowski, T. and Wójcik, A. (2020). A Fuzzy Unscented Kalman Filter in the Adaptive Control System of a Drive System with a Flexible Joint. *Energies*, 13(8), p. 2056. doi: 10.3390/en13082056.

Teixeira, J. E. and Tavares-Lehmann, A. T. C. P. (2022). Industry 4.0 in the European Union: Policies and National Strategies. *Technological Forecasting and Social Change*, 180, p. 121664. doi: 10.1016/j.techfore.2022.121664.

Teolis, A. (1998). *Computational Signal Processing with Wavelets*. Springer, Birkhäuser Boston, MA, USA.

Urbanski, K. and Janiszewski, D. (2021). Position Estimation at Zero Speed for PMSMs Using Artificial Neural Networks. *Energies*, 14(23), p. 8134. doi: 10.3390/en14238134.

Wszołek, G., Czop, P., Słoniewski, J. and Dogrusoz, H. (2020). Vibration Monitoring of CNC Machinery Using MEMS Sensors. *Journal of Vibroengineering*, 22(3), pp. 735–750. doi: 10.21595/jve.2019.20788.